

Mixing angles and electromagnetic properties of ground state pseudoscalar and vector meson nonets in the light-cone quark model

Ho-Meoyng Choi and Chueng-Ryong Ji

Department of Physics, North Carolina State University, Raleigh, N.C. 27695-8202

Abstract

Both the mass spectra and the wave functions of the light pseudoscalar (π, K, η, η') and vector (ρ, K^*, ω, ϕ) mesons are analyzed within the framework of the light-cone constituent quark model. A gaussian radial wave function is used as a trial function of the variational principle for a QCD motivated Hamiltonian which includes not only the Coulomb plus confining potential but also the hyperfine interaction to obtain the correct $\rho - \pi$ splitting. For the confining potential, we use (1) harmonic oscillator potential and (2) linear potential and compare the numerical results for these two cases. The mixing angles of $\omega - \phi$ and $\eta - \eta'$ are predicted and various physical observables such as decay constants, charge radii, and radiative decay rates *etc.* are calculated. Our numerical results in two cases (1) and (2) are overall not much different from each other and have a good agreement with the available experimental data.

12.39.Ki, 13.40.Gp, 13.40.Hq, 14.40.-n

arXiv:hep-ph/9711450v5 8 Jan 1999

I. INTRODUCTION

It has been realized that the relativistic effects are crucial to describe the low-lying hadrons made of u , d and s quarks and anti-quarks [1]. The light-cone quark model [2–12] takes the advantages of the equal light-cone time($\tau = t + z/c$) quantization and includes the important relativistic effects in the hadronic wave functions. The distinct features of the light-cone equal- τ quantization compared to the ordinary equal- t quantization may be summarized as the suppression of vacuum fluctuations with the decoupling of complicated zero-modes and the conversion of the dynamical problem from boost to rotation.

The suppression of vacuum fluctuations is due to the rational energy-momentum dispersion relation which correlates the signs of the light-cone energy $k^- = k^0 - k^3$ and the light-cone momentum $k^+ = k^0 + k^3$ [5]. However, the non-trivial vacuum phenomena can still be realized in the light-cone quantization approach if one takes into account the non-trivial zero-mode($k^+ = 0$) contributions. As an example, it is shown [13] that the axial anomaly in the Schwinger model can be obtained in the light-cone quantization approach by carefully analyzing the contributions from zero-modes. Therefore, in the light-cone quantization approach, one can take advantage of the rational energy-momentum dispersion relation and build a clean Fock state expansion of hadronic wave functions based on a simple vacuum by decoupling the complicated non-trivial zero-modes. The decoupling of zero-modes can be achieved in the light-cone quark model since the constituent quark and anti-quark acquire appreciable constituent masses. Furthermore, the recent lattice QCD results [14] indicated that the mass difference between η' and pseudoscalar octet mesons due to the complicated nontrivial vacuum effect increases(or decreases) as the quark mass m_q decreases(or increases), *i.e.*, the effect of the topological charge contribution should be small as m_q increases. This supports us to build the constituent quark model in the light-cone quantization approach because the complicated nontrivial vacuum effect in QCD can be traded off by the rather large constituent quark masses. One can also provide a well-established formulation of various form factor calculations in the light-cone quantization method using the well-known Drell-Yan-West($q^+ = 0$) frame. We take this as a distinctive advantage of the light-cone quark model.

The conversion of the dynamical problem from boost to rotation can also be regarded as an advantage because the rotation is compact, *i.e.*, closed and periodic. The reason why the rotation is a dynamical problem in the light-cone quantization approach is because the

quantization surface $\tau = 0$ is not invariant under the transverse rotation whose direction is perpendicular to the direction of the quantization axis z at equal τ [15]. Thus, the transverse angular momentum operator involves the interaction that changes the particle number and it is not easy to specify the total angular momentum of a particular hadronic state. Also τ is not invariant under parity [16]. We circumvent these problems of assigning the quantum numbers J^{PC} to hadrons by using the Melosh transformation of each constituents from equal t to equal τ .

In our light-cone quark model of mesons, the meson state $|M \rangle$ is thus represented by

$$|M \rangle = \Psi_{Q\bar{Q}}^M |Q\bar{Q} \rangle, \quad (1.1)$$

where Q and \bar{Q} are the effective dressed quark and anti-quark. The model wave function is given by

$$\Psi_{Q\bar{Q}}^M = \Psi(x, \mathbf{k}_\perp, \lambda_q, \lambda_{\bar{q}}) = \sqrt{\frac{\partial k_n}{\partial x}} \phi(x, \mathbf{k}_\perp) \mathcal{R}(x, \mathbf{k}_\perp, \lambda_q, \lambda_{\bar{q}}), \quad (1.2)$$

where $\phi(x, \mathbf{k}_\perp)$ is the radial wave function, $\partial k_n / \partial x$ is a Jacobi factor and $\mathcal{R}(x, \mathbf{k}_\perp, \lambda_q, \lambda_{\bar{q}})$ is the spin-orbit wave function obtained by the interaction-independent Melosh transformation. When the longitudinal component k_n is defined by $k_n = (x - 1/2)M_0 + (m_q^2 - m_{\bar{q}}^2)/2M_0$, the Jacobian of the variable transformation $\{x, \mathbf{k}_\perp\} \rightarrow \mathbf{k} = (k_n, \mathbf{k}_\perp)$ is given by

$$\frac{\partial k_n}{\partial x} = \frac{M_0}{4x(1-x)} \left\{ 1 - \left[\frac{(m_q^2 - m_{\bar{q}}^2)}{M_0^2} \right]^2 \right\}. \quad (1.3)$$

The explicit spin-orbit wave function of definite spin (S, S_z) can be obtained by

$$\begin{aligned} \mathcal{R}(x, \mathbf{k}_\perp, \lambda_q \lambda_{\bar{q}}) &= \sum_{s_q, s_{\bar{q}}} \langle \lambda_q | \mathcal{R}_M^\dagger(x, \mathbf{k}_\perp, m_q) | s_q \rangle \\ &\times \langle \lambda_{\bar{q}} | \mathcal{R}_M^\dagger(1-x, -\mathbf{k}_\perp, m_{\bar{q}}) | s_{\bar{q}} \rangle < \frac{1}{2} s_q \frac{1}{2} s_{\bar{q}} | S S_z \rangle, \end{aligned} \quad (1.4)$$

where the Melosh transformation is given by

$$\mathcal{R}_M(x, \mathbf{k}_\perp, m) = \frac{m + xM_0 - i\sigma \cdot (\hat{\mathbf{n}} \times \hat{\mathbf{k}})}{\sqrt{(m + xM_0)^2 + \mathbf{k}_\perp^2}} \quad (1.5)$$

with $\hat{\mathbf{n}} = (0, 0, 1)$ being a unit vector in the z -direction.

While the spin-orbit wave function is in principle uniquely determined by the Melosh transformation given by Eq.(1.5), a couple of different schemes for handling the meson mass M_0 in Eq.(1.5) have appeared in the literatures [2–12]. While in the invariant meson mass scheme [2,6–12], the meson mass square M_0^2 is given by

$$M_0^2 = \frac{\mathbf{k}_\perp^2 + m_q^2}{x} + \frac{\mathbf{k}_\perp^2 + m_{\bar{q}}^2}{1-x}, \quad (1.6)$$

in the spin-averaged meson mass scheme [3–5], M_0 was taken as the average of physical masses with appropriate weighting factors from the spin degrees of freedom. Nevertheless, once the best fit parameters were used [5,9], both schemes provided the predictions that were not only pretty similar with each other but also remarkably good [5,7] compared to the available experimental data [17] for form factors, decay constants, charge radii *etc.* of various light pseudoscalar(π, K, η, η') and vector(ρ, K^*, ω, ϕ) mesons as well as their radiative decay widths. The main difference in the best fit parameters was the constituent quark masses, *i.e.*, $m_u = m_d = 330$ MeV, $m_s = 450$ MeV in the spin-averaged meson mass scheme [3–5] while $m_u = m_d = 250$ MeV, $m_s = 370$ MeV in the invariant meson mass scheme [7].

Also, among the literatures [7,8,10] using the invariant meson mass scheme, some literatures [7,8] used the Jacobi factor $\partial k_n / \partial x$ in Eq.(1.2) while some [10] did not. However, we have recently observed [9] that the numerical results of various physical observables from Refs. [7,8] were almost equivalent to those of Ref. [10] regardless of the presence-absence of the Jacobi factor if the same form of radial wave function(*e.g.* Gaussian) was chosen and the best fit model parameters in the radial wave function were used.

However, the effect from the difference in the choice of radial wave function, *e.g.*, harmonic oscillator wave function [7,8,10] versus power-law wave function [11], was so substantial that one could not get the similar result by simply changing the model parameters in the chosen radial wave function. For example, in the phenomenology of various meson radiative decays at low Q^2 , we observed [9] that the gaussian type wave function was clearly better than the power-law wave function in comparison with the available experimental data. On the other hand, the radial function so far has been mostly taken as a model wave function rather than as a solution of QCD motivated dynamical equation. Even though the authors in Ref. [12] adopted the quark potential model developed by Godfrey and Isgur [1] to reproduce the meson mass spectra, their model predictions included neither the mixing angles of $\omega - \phi$ and $\eta - \eta'$ nor the form factors for various radiative decay processes of pseudoscalar and vector mesons.

In this work, we are not taking exactly the same quark potential developed by Godfrey and Isgur [1]. However, we attempt to fill this gap between the model wave function and the QCD motivated potential, which includes not only the Coulomb plus confining potential but also the hyperfine interaction to obtain the correct $\rho - \pi$ splitting. For the confining potential,

we take (1) harmonic oscillator(HO) potential and (2) linear potential and compare the numerical results for these two cases. We use the variational principle to solve the equation of motion. Accordingly, our analysis covers the mass spectra of light pseudoscalar(π, K, η, η') and vector(ρ, K^*, ω, ϕ) mesons and the mixing angles of $\omega - \phi$ and $\eta - \eta'$ as well as other observables such as charge radii, decay constants, radiative decay widths *etc.*. We exploit the invariant meson mass scheme in this model. We also adopt the parametrization to incorporate the quark-annihilation diagrams [18–20] mediated by gluon exchanges and the SU(3) symmetry breaking, *i.e.*, $m_{u(d)} \neq m_s$, in the determination of meson mixing angles.

The paper is organized as follows: In Sec.II, we set up a simple QCD motivated effective Hamiltonian and use the gaussian radial wave function as a trial function of the variational principle. We find the optimum values of the model parameters, quark masses($m_{u(d)}, m_s$) and gaussian parameters($\beta_{u\bar{u}} = \beta_{u\bar{d}} = \beta_{d\bar{d}}, \beta_{u\bar{s}}, \beta_{s\bar{s}}$) for the two cases of confining potentials (1) and (2). We also analyze the meson mass spectra and predict the mixing angles of $\omega - \phi$ and $\eta - \eta'$. We adopt the formulation to incorporate the quark-annihilation diagrams and the effect of SU(3) symmetry breaking in the meson mixing angles. In Sec.III, we calculate the decay constants, charge radii, form factors and radiative decay rates of various light pseudoscalar and vector mesons and discuss the numerical results of the two confining potentials (1) and (2) in comparison with the available experimental data. Summary and discussions follow in Sec.IV. The details of fixing the model parameters and the mixing angle formulations are presented in Appendices A and B, respectively.

II. MODEL DESCRIPTION

The QCD motivated effective Hamiltonian for the description of the meson mass spectra is given by [1,12]

$$\begin{aligned} H_{q\bar{q}}|\Psi_{nlm}^{SS_z}\rangle &= \left[\sqrt{m_q^2 + k^2} + \sqrt{m_{\bar{q}}^2 + k^2} + V_{q\bar{q}} \right] |\Psi_{nlm}^{SS_z}\rangle, \\ &= \left[H_0 + V_{q\bar{q}} \right] |\Psi_{nlm}^{SS_z}\rangle = M_{q\bar{q}} |\Psi_{nlm}^{SS_z}\rangle, \end{aligned} \quad (2.1)$$

where $M_{q\bar{q}}$ is the mass of the meson, $k^2 = \mathbf{k}_\perp^2 + k_n^2$, and $|\Psi_{nlm}^{SS_z}\rangle$ is the meson wave function given in Eq.(1.2). In this work, we use the two interaction potentials $V_{q\bar{q}}$ for the pseudoscalar(0^{-+}) and vector(1^{--}) mesons:(1) Coulomb plus harmonic oscillator(HO), and (2) Coulomb plus linear confining potentials. In addition, the hyperfine interaction, which is essential to distinguish vector from pseudoscalar mesons, is included for both cases, *viz.*

$$\begin{aligned}
V_{q\bar{q}} &= V_0(r) + V_{\text{hyp}}(r) \\
&= a + \mathcal{V}_{\text{conf.}} - \frac{4\kappa}{3r} + \frac{2\vec{S}_q \cdot \vec{S}_{\bar{q}}}{3m_q m_{\bar{q}}} \nabla^2 V_{\text{Coul}},
\end{aligned} \tag{2.2}$$

where $\mathcal{V}_{\text{conf.}} = br[r^2]$ for the linear[HO] potential and $\langle \vec{S}_q \cdot \vec{S}_{\bar{q}} \rangle = 1/4[-3/4]$ for vector[pseudoscalar] meson. Even though more realistic solution of Eq.(2.1) can be obtained by expanding the radial function $\phi_{n,l=0}(k^2)$ onto a truncated set of HO basis states [1,12], *i.e.*, $\sum_{n=1}^{n_{\text{max}}} c_n \phi_{n,0}(k^2)$, our intention in this work is to explore only the 0^{-+} and 1^{-} ground state meson properties. Therefore, we use the $1S$ state harmonic wave function $\phi_{10}(k^2)$ as a trial function of the variational principle

$$\phi_{10}(x, \mathbf{k}_{\perp}) = \left(\frac{1}{\pi^{3/2} \beta^3} \right)^{1/2} \exp(-k^2/2\beta^2), \tag{2.3}$$

where $\phi(x, \mathbf{k}_{\perp})$ is normalized according to

$$\sum_{\nu\bar{\nu}} \int_0^1 dx \int d^2\mathbf{k}_{\perp} |\Psi_{100}^{S\bar{S}z}(x, \mathbf{k}_{\perp}, \nu\bar{\nu})|^2 = \int_0^1 dx \int d^2\mathbf{k}_{\perp} \frac{\partial k_n}{\partial x} |\phi_{10}(x, \mathbf{k}_{\perp})|^2 = 1. \tag{2.4}$$

Because of this rather simple trial function, our results could be regarded as crude approximations. However, we note that this choice is consistent with the light-cone quark model wave function which has been quite successful in describing various meson properties [3–10]. Furthermore, Eq.(2.3) takes the same form as the ground state solution of the HO potential even though it is not the exact solution for the linear potential case. As we show in Appendix A, after fixing the parameters a, b and κ , the Coulomb plus HO potential $V_0(r)$ in Eq.(2.2), turns out to be very similar in the relevant range of potential ($r \lesssim 2$ fm) to the Coulomb plus linear confining potentials[see Figs.1(a) and 1(b)] which are frequently used in the literatures [1,12,21–25]. The details of fixing the parameters of our model, *i.e.*, quark masses($m_{u(d)}, m_s$), gaussian parameters($\beta_{u\bar{d}}, \beta_{u\bar{s}}, \beta_{s\bar{s}}$) and potential parameters (a, b, κ) in $V_{q\bar{q}}$ given by Eq.(2.2) are summarized in the Appendix A.

Following the procedure listed in the Appendix A, our optimized model parameters are given in Table I. In fixing all of these parameters, the variational principle[Eq.(A1)] plays the crucial role for $u\bar{d}, u\bar{s}$, and $s\bar{s}$ meson systems to share the same potential parameters (a, b, κ) regardless of their quark-antiquark contents[see Figs.2(a) and 2(b)].

We also determine the mixing angles from the mass spectra of (ω, ϕ) and (η, η') . Identifying $(f_1, f_2) = (\phi, \omega)$ and (η, η') for vector and pseudoscalar nonets, the physical meson states f_1 and f_2 are given by

$$\begin{aligned}
|f_1\rangle &= -\sin\delta|n\bar{n}\rangle - \cos\delta|s\bar{s}\rangle, \\
|f_2\rangle &= \cos\delta|n\bar{n}\rangle - \sin\delta|s\bar{s}\rangle,
\end{aligned}
\tag{2.5}$$

where $|n\bar{n}\rangle \equiv 1/\sqrt{2}|u\bar{u} + d\bar{d}\rangle$ and $\delta = \theta_{SU(3)} - 35.26^\circ$ is the mixing angle. Taking into account SU(3) symmetry breaking and using the parametrization for the (mass)² matrix suggested by Scadron [20], we obtain

$$\tan^2\delta = \frac{(M_{f_2}^2 - M_{n\bar{n}}^2)(M_{s\bar{s}}^2 - M_{f_1}^2)}{(M_{f_2}^2 - M_{s\bar{s}}^2)(M_{f_1}^2 - M_{n\bar{n}}^2)},
\tag{2.6}$$

which is the model independent equation for any meson $q\bar{q}$ nonets. The details of obtaining meson mixing angles using quark-annihilation diagrams are summarized in the Appendix B. In order to predict the $\omega - \phi$ and $\eta - \eta'$ mixing angles, we use the physical masses [17] of $M_{f_1} = (m_\phi, m_\eta)$ and $M_{f_2} = (m_\omega, m_{\eta'})$ as well as the masses of $M_{s\bar{s}}^V = 996$ [952] MeV and $M_{s\bar{s}}^P = 732$ [734] MeV obtained from the expectation value of $H_{s\bar{s}}$ in Eq.(2.1) for HO[linear] potential case[see Appendix A for more details]. Our predictions for $\omega - \phi$ and $\eta - \eta'$ mixing angles for HO[linear] potential are $|\delta_V| \approx 4.2^\circ$ [7.8°] and $\theta_{SU(3)} \approx -19.3^\circ$ [-19.6°], respectively. The used mass spectra of light pseudoscalar and vector mesons are summarized in Table II. Since the signs of δ_V for $\omega - \phi$ mixing are not yet definite [18–20,27–29] in the analysis of the quark-annihilation diagram[see Appendix B], we will keep both signs of δ_V when we compare various physical observables in the next section.

III. APPLICATION

In this section, we now use the optimum model parameters presented in the previous section and calculate various physical observables; (1) decay constants of light pseudoscalar and vector mesons, (2) charge radii of pion and kaon, (3) form factors of neutral and charged kaons, and (4) radiative decay widths for the $V(P) \rightarrow P(V)\gamma$ and $P \rightarrow \gamma\gamma$ transitions. These observables are calculated for the two potentials(HO and linear) to gauge the sensitivity of our results.

Our calculation is carried out using the standard light-cone frame($q^+ = q^0 + q^3 = 0$) with $\mathbf{q}_\perp^2 = Q^2 = -q^2$. We think that this is a distinct advantage in the light-cone quark model because various form factor formulations are well established in the light-cone quantization method using this well-known Drell-Yan-West frame($q^+ = 0$). The charge form factor of the pseudoscalar meson can be expressed for the ‘+’-component of the current J^μ as follows

$$F(Q^2) = e_q I(Q^2, m_q, m_{\bar{q}}) + e_{\bar{q}} I(Q^2, m_{\bar{q}}, m_q), \quad (3.1)$$

where $e_q(e_{\bar{q}})$ is the charge of quark(anti-quark) and

$$I(Q^2, m_q, m_{\bar{q}}) = \int_0^1 dx \int d^2\mathbf{k}_\perp \sqrt{\frac{\partial k_n}{\partial x}} \phi(x, \mathbf{k}_\perp) \sqrt{\frac{\partial k'_n}{\partial x}} \phi^*(x, \mathbf{k}'_\perp) \frac{\mathcal{A}^2 + \mathbf{k}_\perp \cdot \mathbf{k}'_\perp}{\sqrt{\mathcal{A}^2 + \mathbf{k}_\perp^2} \sqrt{\mathcal{A}^2 + \mathbf{k}'_\perp^2}}, \quad (3.2)$$

with the definition of \mathcal{A} and \mathbf{k}'_\perp given by

$$\mathcal{A} = xm_{\bar{q}} + (1-x)m_q, \quad \mathbf{k}'_\perp = \mathbf{k}_\perp + (1-x)\mathbf{q}_\perp. \quad (3.3)$$

Subsequently, the charge radius of the meson can be calculated by $r^2 = -6dF(Q^2)/dQ^2|_{Q^2=0}$. Also, the decay constant f_P of the pseudoscalar meson($P = \pi, K$) is given by

$$f_P = \frac{\sqrt{6}}{(2\pi)^{3/2}} \int_0^1 dx \int d^2\mathbf{k}_\perp \sqrt{\frac{\partial k_n}{\partial x}} \phi(x, \mathbf{k}_\perp) \frac{\mathcal{A}}{\sqrt{\mathcal{A}^2 + \mathbf{k}_\perp^2}}. \quad (3.4)$$

Since all other formulae for the physical observables such as the vector meson decay constants f_V of $V \rightarrow e^+e^-$, decay rates for the $V(P) \rightarrow P(V)\gamma$ and $P \rightarrow \gamma\gamma$ transitions have already been given in our previous publication [5] and also in other references(*e.g.* Ref. [7]), we do not list them here again. The readers are recommended to look at Refs. [5] and [7] for the details of unlisted formulae. In Fig.3, we show our numerical results of the pion form factor for HO(solid line) and linear(dotted line) cases and compare with the available experimental data [30] up to $Q^2 \sim 8 \text{ GeV}^2$ region. Since our model parameters of $m_u = 0.25 \text{ GeV}$ and $\beta_{u\bar{u}} = 0.3194 \text{ GeV}$ for the HO case are same with the ones used in Refs. [7] and [11], our numerical result of the pion form factor is identical with the Fig.2(solid line) in Ref. [11]. In Figs.4(a) and 4(b), we show our numerical results for the form factors of the charged and neutral kaons and compare with the results of vector model dominance(VMD) [31], where a simple two-pole model of the kaon form factors was assumed, *i.e.*, $F_{K+(K^0)}(Q^2) = e_{u(d)}m_\omega^2/(m_\omega^2 + Q^2) + e_{\bar{s}}m_\phi^2/(m_\phi^2 + Q^2)$. From Figs.4(a) and 4(b), we can see that the neutral kaon form factors using the model parameters obtained from HO and linear potentials are not much different from each other even though the charged ones are somewhat different.

The decay constants and charge radii of various pseudoscalar and vector mesons for the two potential cases are given in Table III and compared with experimental data [17,32]. While our optimal prediction of δ_V was $|\delta_V| = 4.2^\circ [7.8^\circ]$ for HO[linear] potential model, we displayed our results for the common δ_V value with a small variation (*i.e.*, $|\delta_V| = 3.3^\circ \pm 1^\circ$) in Table III to show the sensitivity. The results for both potentials are not much different

from each other and both results are quite comparable with the experimental data. The decay widths of the $V(P) \rightarrow P(V)\gamma$ transitions are also given for the two different potential models in Table IV. Although it is not easy to see which sign of δ_V for HO potential model is more favorable to the experimental data, the positive sign of δ_V looks a little better than the negative one for the processes of $\omega(\phi) \rightarrow \eta\gamma$ and $\eta' \rightarrow \omega\gamma$ transitions. Especially, the overall predictions of HO potential model with the positive δ_V seem to be in a good agreement with the experimental data. However, more observables should be compared with the data in order to give more definite answer for this sign issue of $\omega - \phi$ mixing angle. The overall predictions of linear potential model are also comparable with the experimental data even though the large variation of the mixing angle δ_V should be taken into account in this case.

In Table V, we show the results of $P(= \pi, \eta, \eta') \rightarrow \gamma\gamma$ decay widths obtained from our two potential models with the axial anomaly plus partial conservation of the axial current(PCAC) relations. The predictions of $\eta(\eta') \rightarrow \gamma\gamma$ decay widths using PCAC are in a good agreement with the experimental data for both HO and linear potential models with $\eta - \eta'$ mixing angle, $\theta_{SU(3)} = -19^\circ$. The predictions of the decay constants for the octet and singlet mesons, *i.e.*, η_8 and η_0 , are $f_8/f_\pi = 1.254[1.324]$ and $f_0/f_\pi = 1.127[1.162]$ MeV for HO[linear] potential model, respectively. Our predictions of f_8 and f_0 are not much different from the predictions of chiral perturbation theory [33] reported as $f_8/f_\pi = 1.25$ and $f_0/f_\pi = 1.04 \pm 0.04$, respectively. Another important mixing-independent quantity related to f_8 and f_0 is the R -ratio defined by

$$R \equiv \left[\frac{\Gamma(\eta \rightarrow \gamma\gamma)}{m_\eta^3} + \frac{\Gamma(\eta' \rightarrow \gamma\gamma)}{m_{\eta'}^3} \right] \frac{m_\pi^3}{\Gamma(\pi \rightarrow \gamma\gamma)} = \frac{1}{3} \left(\frac{f_\pi^2}{f_8^2} + 8 \frac{f_\pi^2}{f_0^2} \right). \quad (3.5)$$

Our predictions, $R = 2.31$ and 2.17 for HO and linear potential model cases, respectively, are quite comparable to the available experimental data [34,35], $R_{\text{exp}} = 2.5 \pm 0.5(\text{stat}) \pm 0.5(\text{sys})$. Also, the Q^2 -dependent decay rates $\Gamma_{P\gamma}(Q^2)$ are calculated from the usual one-loop diagram [5,7] and the results are shown in Figs.5-7. Our results for both potential models are not only very similar with each other but also in a remarkably good agreement with the experimental data [36–38] up to $Q^2 \sim 10 \text{ GeV}^2$ region. We think that the reason why our model is so successful for $P \rightarrow \gamma^*\gamma$ transition form factors is because the Q^2 -dependence ($\sim 1/Q^2$) is due to the off-shell quark propagator in the one-loop diagram and there is no angular condition [5] associated with the pseudoscalar meson.

IV. SUMMARY AND DISCUSSIONS

In the light-cone quark model approach, we have investigated the mass spectra, mixing angles, and other physical observables of light pseudoscalar and vector mesons using QCD motivated potentials given by Eq.(2.2). The variational principle for the effective Hamiltonian is crucial to find the optimum values of our model parameters. As shown in Figs.1(a) and 1(b), we noticed that both central potentials in Eq.(2.2) are not only very similar to each other but also quite close to the ISGW2 [25] model potentials. In Figs.1(a) and 1(b), we have also included the GI potential for comparison. Using the physical masses of (ω, ϕ) and (η, η') , we were able to predict the $\omega - \phi$ and $\eta - \eta'$ mixing angles as $|\delta_V| \approx 4.2^\circ [7.8^\circ]$ and $\theta_{SU(3)} \approx -19.3^\circ [-19.6^\circ]$ for the HO[linear] potential model, respectively. We also have checked that the sensitivity of the mass spectra of (ω, ϕ) to $\sim 1^\circ [5^\circ]$ variation of δ_V , *i.e.*, from $\delta_V = 4.2^\circ [7.8^\circ]$ to 3.3° for HO[linear] potential case, is within 1%[5%] level.

Then, we applied our models to compute the observables such as charge radii, decay constants, and radiative decays of $P(V) \rightarrow V(P)\gamma^*$ and $P \rightarrow \gamma\gamma^*$. As summarized in Tables III, IV, and V, our numerical results for these observables in the two cases(HO and linear) are overall not much different from each other and are in a rather good agreement with the available experimental data [17]. Furthermore, our results of the R -ratio presented in Eq.(3.5) are in a good agreement with the experimental data [34,35]. The Q^2 dependence of $P \rightarrow \gamma\gamma^*$ processes were also compared with the experimental data up to $Q^2 \sim 8 \text{ GeV}^2$. The Q^2 -dependence for these processes is basically given by the off-shell quark propagator in the one-loop diagrams. As shown in Figs.5-7, our results are in an excellent agreement with the experimental data [36–38]. Both the pion and kaon form factors were also predicted in Figs.3 and 4, respectively. We believe that the success of light-cone quark model hinges upon the suppression of complicated zero-mode contributions from the light-cone vacuum due to the rather large constituent quark masses. The well-established formulation of form factors in the Drell-Yan-West frame also plays an important role for our model to provide comparable result with the experimental data. Because of these successful applications of our variational effective Hamiltonian method, the extension to the heavy(b and c quark sector) pseudoscalar and vector mesons and the 0^{++} scalar mesons is currently under consideration.

While there have been previous light-cone quark model results on the observables that we calculated in this work, they were based on the approach of modeling the wavefunction rather than modeling the potential. Our approach in this work attempting to fill the gap

between the model wavefunction and the QCD motivated potential has not yet been explored to cover as many observables as we did in this work. Nevertheless, it is not yet clear which sign of $\omega - \phi$ mixing angle should be taken, even though the overall agreement between our HO potential model with the positive sign, *i.e.*, $\delta_V \sim 3.3^\circ$ and the available experimental data seems to be quite good. If we were to choose the sign of X as $X > 0$ in Eq.(B4), then the fact that the mass difference $m_\omega - m_\rho$ is positive is correlated with the sign of the $\omega - \phi$ mixing angle [39]. In other words, $m_\omega > m_\rho$ implies $\delta_V > 0$ from Eqs.(B3)-(B5). Perhaps, the precision measurement of $\phi \rightarrow \eta'\gamma$ envisioned in the future at TJNAF experiment might be helpful to give more stringent test of δ_V . In any case, more observables should be compared with the experimental data to give more definite assessment on this sign issue.

ACKNOWLEDGMENTS

We are grateful to Prof. Nathan Isgur for his careful reading of this paper and providing useful information on the sign issue of the $\omega - \phi$ mixing. This work was supported by the Department of Energy under DE-FG02-96ER40947. The North Carolina Supercomputing Center and the National Energy Research Scientific Computer Center are also acknowledged for the grant of supercomputer time.

APPENDIX A: FIXATION OF THE MODEL PARAMETERS USING THE VARIATIONAL PRINCIPLE

In this Appendix A, we discuss how to fix the parameters of our model, *i.e.*, quark masses(m_u, m_s), gaussian parameters($\beta_{u\bar{u}} = \beta_{u\bar{d}}, \beta_{u\bar{s}}, \beta_{s\bar{s}}$) and potential parameters (a, b, κ) in $V_{q\bar{q}}$ given by Eq.(2.2). In our potential model, the $\rho - \pi$ mass splitting is obtained by the hyperfine interaction, V_{hyp} .

Our variational method first evaluates $\langle \Psi|[H_0 + V_0]|\Psi \rangle$ with a trial function $\phi_{10}(k^2)$ that depends on the parameters (m, β) and varies these parameters until the expectation value of $H_0 + V_0$ is a minimum. Once these model parameters are fixed, then, the mass eigenvalue of each meson is obtained by $M_{q\bar{q}} = \langle \Psi|[H_0 + V_0]|\Psi \rangle + \langle \Psi|H_{\text{hyp}}|\Psi \rangle$ ¹. In this approach, we do not discriminate the gaussian parameter set $\beta = (\beta_{u\bar{u}}, \beta_{u\bar{s}}, \beta_{s\bar{s}})$ by the spin structure of mesons.

Let us now illustrate our detailed procedures of finding the optimized values of the model parameters using the variational principle:

$$\frac{\partial \langle \Psi|[H_0 + V_0]|\Psi \rangle}{\partial \beta} = 0. \quad (\text{A1})$$

From Eqs.(2.1)-(2.2) and Eq.(A1), we obtain the following equations for HO and linear potentials:

$$\text{H.O. potential : } b_h = \frac{\beta^3}{3} \left\{ \frac{\partial \langle \Psi|H_0|\Psi \rangle}{\partial \beta} - \frac{8\kappa_h}{3\sqrt{\pi}} \right\}, \quad (\text{A2})$$

$$\text{Linear potential : } b_l = \frac{\sqrt{\pi}\beta^2}{2} \left\{ \frac{\partial \langle \Psi|H_0|\Psi \rangle}{\partial \beta} - \frac{8\kappa_l}{3\sqrt{\pi}} \right\}, \quad (\text{A3})$$

where the subscript $h[l]$ represents the HO[linear] potential parameters. Eqs.(A2) and (A3) imply that the variational principle reduces a degree of freedom in the parameter space. Thus, we have now four parameters, *i.e.*, $\{m_u, \beta_{u\bar{d}}, a, \kappa(\text{or } b)\}$. However, in order to determine these four parameters from the two experimental values of ρ and π masses, we need to choose two input parameters. These two parameters should be carefully chosen. Otherwise, even though the other two parameters are fixed by fitting the ρ and π masses, our predictions would be poor for other observables such as the ones in Sec.III as well as other mass spectra. From our trial and error type of analyses, we find that $m_u = 0.25[0.22]$ GeV

¹As we will see later, in our fitting of the $\rho - \pi$ splitting, the rather big mass shift due to the hyperfine interaction is attributed to the large QCD coupling constant, $\kappa = 0.3 \sim 0.6$.

is the best input quark mass parameter for the HO[linear] potential among the widely used $u(d)$ quark mass, $m_u = 0.22$ GeV [1], 0.25 GeV [7], and 0.33 GeV [3,24,25]. For the linear potential, the string tension $b_l = 0.18$ GeV² is well known from other quark model analyses [1,24,25] commensurate with Regge phenomenology. Thus, we take $m_u = 0.22$ GeV and $b_l = 0.18$ GeV² as our input parameters for the linear potential case. However, for the HO potential, there is no well-known quantity corresponding to the string tension and thus we use the parameters of $m_{u(d)} = 0.25$ GeV and $\beta_{u\bar{d}} = 0.3194$ GeV as our input parameters which turn out to be good values to describe various observables of both the π and ρ mesons for the gaussian radial wave function [7].

Using Eqs.(2.1),(A2) and (A3) with the input value sets of (1)($m_u=0.25$ GeV, $\beta_{u\bar{d}}=0.3194$ GeV) for the HO potential and (2)($m_u = 0.22$ GeV, $b_l = 0.18$ GeV²) for the linear potential, we obtain the following parameters from the ρ and π masses, viz., $\langle \Psi | H_{u\bar{d}}^{V(P)} | \Psi \rangle = M_{u\bar{d}}^{V(P)} = m_{\rho(\pi)}$ (P = Pseudoscalar and V = Vector):

$$(1) \text{ H.O. potential : } a_h = -0.144 \text{ GeV, } b_h = 0.010 \text{ GeV}^3, \quad \kappa_h = 0.607, \quad (\text{A4})$$

$$(2) \text{ Linear potential : } a_l = -0.724 \text{ GeV, } \beta_{u\bar{d}} = 0.3659 \text{ GeV, } \quad \kappa_l = 0.313. \quad (\text{A5})$$

As shown in Fig.1(a), it is interesting to note that our two central potentials, Coulomb plus HO(solid line) and Coulomb plus linear (dotted line) potentials, are not much different from each other and furthermore quite comparable to the Coulomb plus linear quark potential model suggested by Scora-Isgur(ISGW2) [25](long-dashed line for $\kappa = 0.3$ and dot-dashed line for $\kappa = 0.6$) up to the range of $r \lesssim 2$ fm. Those four potentials(H.O., Linear, and ISGW2) are also compared with the Godfrey and Isgur(GI) potential model [1](short-dashed line) in Fig.1(a). The corresponding string tensions, *i.e.*, $f_0(r) = -dV_0(r)/dr$, are also shown in Fig.1(b).

Next, among various sets of $\{m_s, \beta_{u\bar{s}}\}$ satisfying Eqs.(A2) and (A3), we find $m_s = 0.48[0.45]$ GeV and $\beta_{u\bar{s}} = 0.3419[0.3886]$ GeV for HO[linear] potential by fitting optimally the masses of K^* and K , *i.e.*, $M_{u\bar{s}}^{V(P)} = m_{K^*(K)}$. Once the set of $\{m_s, \beta_{u\bar{s}}\}$ is fixed, then the parameters, $\beta_{s\bar{s}} = 0.3681[0.4128]$ GeV for HO[linear] potential, can be obtained from Eq.(A2)[(A3)]. Subsequently, $M_{s\bar{s}}^V$ and $M_{s\bar{s}}^P$ are predicted as $996[952]$ MeV and $732[734]$ MeV for HO[linear] potential, respectively. As shown in Fig.2(a)[2(b)], the solid, dotted and dot-dashed lines are fixed by the HO[linear] potential parameter sets of $\{m_u, \beta_{u\bar{d}}\}$, $\{m_s, \beta_{u\bar{s}}\}$, and $\beta_{s\bar{s}}$, respectively, and these three lines cross the same point in the space of b and κ if the parameters in Table I are used.

We have also examined the sensitivity of our variational parameters and the corresponding mass spectra using a gaussian smearing function to weaken the singularity of $\delta^3(r)$ in hyperfine interaction, viz.,

$$\delta^3(r) \rightarrow \frac{\sigma^3}{\pi^{3/2}} \exp(-\sigma^2 r^2). \quad (\text{A6})$$

By adopting the well-known cut-off value of $\sigma = 1.8$ [1,26] and repeating the same optimization procedure as the contact term (*i.e.*, $\delta^3(r)$) case, we obtain the following parameters² for each potential:

$$\text{H.O. potential : } a_h = -0.123 \text{ GeV}, \quad b_h = 9.89 \times 10^{-3} \text{ GeV}^3, \quad \kappa_h = 0.636, \quad (\text{A7})$$

$$\text{Linear potential : } a_l = -0.7 \text{ GeV}, \quad b_l = 0.176 \text{ GeV}^2, \quad \kappa_l = 0.332. \quad (\text{A8})$$

The changes of other model parameters and mass spectra are given in Tables I and II. As one can see in Eqs.(A7)-(A8) and Tables I-II, the effects of smearing out $\delta^3(r)$ are quite small and the smearing effects are in fact negligible for our numerical analysis in Sec.III.

APPENDIX B: MIXING ANGLES OF (η, η') AND (ω, ϕ)

In this appendix, we illustrate the mixing angles of (η, η') and (ω, ϕ) by adopting the formulation to incorporate the quark-annihilation diagrams and the effect of SU(3) symmetry breaking in the meson mixing angles.

The Eq.(2.5) satisfy the (mass)² eigenvalue equation

$$\mathcal{M}^2 |f_i\rangle = M_{f_i}^2 |f_i\rangle \quad (i = 1, 2). \quad (\text{B1})$$

Taking into account SU(3) symmetry breaking, we use the following parametrization for \mathcal{M}^2 suggested by Scadron [20]

$$\mathcal{M}^2 = \begin{pmatrix} M_{n\bar{n}}^2 + 2\lambda & \sqrt{2}\lambda X \\ \sqrt{2}\lambda X & M_{s\bar{s}}^2 + \lambda X^2 \end{pmatrix}. \quad (\text{B2})$$

The parameter λ characterizes the strength of the quark-annihilation graph which couples the $I=0$ $u\bar{u}$ state to $I=0$ $u\bar{u}, d\bar{d}, s\bar{s}$ states with equal strength in the exact SU(3) limit.

²For the sensitivity check of smearing out $\delta^3(r)$ [Eq.(A6)], we kept $\beta_{u\bar{d}} = 0.3659$ GeV for the linear potential case given by Eq.(A5) as an input value and checked how much b_l changed.

The parameter X , however, pertains to SU(3) symmetry breaking such that the quark-annihilation graph factors into its flavor parts, with λ , λX and λX^2 for the $u\bar{u} \rightarrow u\bar{u}(d\bar{d})$, $u\bar{u} \rightarrow s\bar{s}$ (or $s\bar{s} \rightarrow u\bar{u}$), and $s\bar{s} \rightarrow s\bar{s}$ processes, respectively. Of course, $X \rightarrow 1$ in the SU(3) exact limit. Also, in Eq.(B2), $M_{n\bar{n}}^2$ and $M_{s\bar{s}}^2$ describe the masses of the corresponding mesons in the absence of mixing.

Solving Eqs.(2.5),(B1), and (B2), we obtain Eq.(2.6) and

$$\lambda = \frac{(M_{f_1}^2 - M_{n\bar{n}}^2)(M_{f_2}^2 - M_{n\bar{n}}^2)}{2(M_{s\bar{s}}^2 - M_{n\bar{n}}^2)}, \quad (\text{B3})$$

$$X^2 = \frac{2(M_{f_2}^2 - M_{s\bar{s}}^2)(M_{s\bar{s}}^2 - M_{f_1}^2)}{(M_{f_2}^2 - M_{n\bar{n}}^2)(M_{f_1}^2 - M_{n\bar{n}}^2)}, \quad (\text{B4})$$

$$\tan 2\delta = \frac{2\sqrt{2}\lambda X}{(M_{s\bar{s}}^2 - M_{n\bar{n}}^2 + \lambda X^2 - 2\lambda)}. \quad (\text{B5})$$

The Eqs.(B3) and (B4) are identical to the two constraints, $\text{Tr}(\mathcal{M}^2) = \text{Tr}(M_{f_i}^2)$ and $\det(\mathcal{M}^2) = \det(M_{f_i}^2)$. The sign of δ is fixed by the signs of the λ and X from Eq.(B5). Also, since Eq.(B2) is decoupled from the subspace of $(u\bar{u} - d\bar{d})/\sqrt{2}$, the physical masses of m_π and m_ρ are confirmed to be the masses of $M_{n\bar{n}}^P$ and $M_{n\bar{n}}^V$, respectively, as we used in Sec.II to fix the parameters (a, b, κ) .

Given the fixed physical masses of $M_{n\bar{n}}^P = m_\pi$ and $M_{n\bar{n}}^V = m_\rho$ together with $M_{f_i}(i = 1, 2)$, the magnitudes of mixing angles for $\eta - \eta'$ and $\omega - \phi$ now depend only on the masses of $M_{s\bar{s}}^P$ and $M_{s\bar{s}}^V$, respectively, from Eq.(2.5). However, from Eqs.(B3)-(B5), one can see that the sign of mixing angle depends on the sign of parameter X . While $X_P > 0$ is well supported by the particle data group [17] ($-23^\circ \lesssim \theta_{SU(3)}^{\eta-\eta'} \lesssim -10^\circ$), the sign of X_V is not yet definite at the present stage of phenomenology. Regarding on the sign of X_V , it is interesting to note that $\delta_V \approx -3.3^\circ (= \theta_{SU(3)} - 35.26^\circ)$ (*i.e.*, $X_V < 0$) is favored in Refs. [7,27–29], while the conventional Gell-Mann-Okubo mass formula for the exact SU(3) limit ($X \rightarrow 1$) predicts $\delta_V \approx 0^\circ$ in the linear mass scheme and $\delta_V \approx +3.3^\circ$ (*i.e.*, $X_V > 0$) in the quadratic mass scheme [17]. Our predictions for the $\omega - \phi$ and $\eta - \eta'$ mixing angles are given in Sec.II.

The corresponding results of the mixing parameters $\lambda_{V(P)}$ and $X_{V(P)}$ in Eqs.(B3) and (B4) are obtained for the HO[linear] potential as follows

$$\begin{aligned} \lambda_V &= 0.57[0.73]m_\pi^2 \text{ GeV}^2, & X_V &= \pm 2.10[\pm 3.08], \\ \lambda_P &= 13.5[13.3]m_\pi^2 \text{ GeV}^2, & X_P &= 0.84[0.85]. \end{aligned} \quad (\text{B6})$$

Our values of λ_V and λ_P for both HO and linear potential cases are not much different from the predictions of Ref. [20]. The reason why λ_V is much smaller than λ_P , *i.e.*, $\lambda_P \approx 23[18]\lambda_V$

in our HO[linear] case and $\lambda_P \approx 18\lambda_V$ in Ref. [20], may be attributed to the fact that in the quark-annihilation graph, the 1^{--} annihilation graph involves one more gluon compared to the 0^{-+} annihilation graph. This also indicates the strong departure of $\eta - \eta'$ from the ideal mixing.

TABLES

TABLE I. Optimized quark masses (m_q, m_s) and the gaussian parameters β for both harmonic oscillator and linear potentials obtained from the variational principle. $q=u$ and d .

Potential	m_q [GeV]	m_s [GeV]	$\beta_{q\bar{q}}$ [GeV]	$\beta_{s\bar{s}}$ [GeV]	$\beta_{q\bar{s}}$ [GeV]
H.O.	0.25	0.48	0.3194	0.3681[0.3703] ^[a]	0.3419[0.3428]
Linear	0.22	0.45	0.3659	0.4128[0.4132]	0.3886[0.3887]

^[a] The values in parentheses are results from the smearing function [1,26] in Eq.(A6) instead of the contact term.

TABLE II. Fit of the ground state meson masses with the parameters given in Table I. Underline masses are input data. The masses of (η, η') and (ω, ϕ) were used to determine the mixing angles of $\eta - \eta'$ and $\omega - \phi$, respectively.

¹ S_0	Experiment[MeV]	H.O.	Linear	³ S_1	Experiment	H.O.	Linear
π	135±0.00035	<u>135</u>	<u>135</u>	ρ	770± 0.8	<u>770</u>	<u>770</u>
K	494± 0.016	470[469] ^[b]	478[478]	K^*	892± 0.24	875[875]	850[850]
η	547± 0.19	<u>547</u>	<u>547</u>	ω	782± 0.12	<u>782</u>	<u>782</u>
η'	958±0.14	<u>958</u>	<u>958</u>	ϕ	1020±0.008	<u>1020</u>	<u>1020</u>

^[b] The values in parentheses are results from the smearing function in Eq.(A6) instead of the contact term.

TABLE III. Decay constants and charge radii for various pseudoscalar and vector mesons. For comparison, we use $|\delta_V| = 3.3^\circ \pm 1^\circ$ for both potential cases. The experimental data are taken from Ref.[17], unless otherwise noted.

Observables	$\delta_V = -3.3^\circ \pm 1^\circ$		$\delta_V = +3.3^\circ \pm 1^\circ$		Experiment
	H.O.	Linear	H.O.	Linear	
f_π [MeV]	92.4	91.8	92.4	91.8	92.4 ± 0.25
f_K [MeV]	109.3	114.1	109.3	114.1	113.4 ± 1.1
f_ρ [MeV]	151.9	173.9	151.9	173.9	152.8 ± 3.6
f_{K^*} [MeV]	157.6	180.8	157.6	180.8	—
f_ω [MeV]	45.9 ± 1.4	52.6 ± 1.6	55.1 ± 1.3	63.1 ± 1.5	45.9 ± 0.7
f_ϕ [MeV]	82.6 ∓ 0.8	94.3 ∓ 0.9	76.7 ∓ 1.0	87.6 ∓ 1.1	79.1 ± 1.3
r_π^2 [fm ²]	0.449	0.425	0.449	0.425	0.432 ± 0.016 [32]
$r_{K^+}^2$ [fm ²]	0.384	0.354	0.384	0.354	0.34 ± 0.05 [32]
$r_{K^0}^2$ [fm ²]	-0.091	-0.082	-0.091	-0.082	-0.054 ± 0.101 [32]

TABLE IV. Radiative decay widths for the $V(P) \rightarrow P(V)\gamma$ transitions. The mixing angles, $\theta_{SU(3)} = -19^\circ$ for $\eta - \eta'$ and $|\delta_V| = 3.3^\circ \pm 1^\circ$ for $\omega - \phi$, are used for both potential models, respectively. The experimental data are taken from Ref.[17].

Widths	$\delta_V = -3.3^\circ \pm 1^\circ$		$\delta_V = +3.3^\circ \pm 1^\circ$		Experiment[keV]
	H.O.	Linear	H.O.	Linear	
$\Gamma(\rho^\pm \rightarrow \pi^\pm \gamma)$	76	69	76	69	68 ± 8
$\Gamma(\omega \rightarrow \pi \gamma)$	730 ± 1.3	667 ± 1.3	730 ∓ 1.3	667 ∓ 1.3	717 ± 51
$\Gamma(\phi \rightarrow \pi \gamma)$	$5.6_{+3.9}^{-2.9}$	$5.1_{+3.6}^{-2.6}$	$5.6_{-2.9}^{+3.9}$	$5.1_{-2.6}^{+3.6}$	5.8 ± 0.6
$\Gamma(\rho \rightarrow \eta \gamma)$	59	54	59	54	58 ± 10
$\Gamma(\omega \rightarrow \eta \gamma)$	8.7 ∓ 0.3	7.9 ∓ 0.3	6.9 ∓ 0.3	6.3 ∓ 0.3	7.0 ± 1.8
$\Gamma(\phi \rightarrow \eta \gamma)$	38.7 ± 1.6	37.8 ± 1.5	49.2 ± 1.6	47.6 ± 1.5	55.8 ± 3.3
$\Gamma(\eta' \rightarrow \rho \gamma)$	68	62	68	62	61 ± 8
$\Gamma(\eta' \rightarrow \omega \gamma)$	4.9 ± 0.4	4.5 ± 0.4	7.6 ± 0.4	7.0 ± 0.4	6.1 ± 1.1
$\Gamma(\phi \rightarrow \eta' \gamma)$	0.41 ∓ 0.01	0.39 ∓ 0.01	0.36 ∓ 0.01	0.34 ∓ 0.01	< 1.8
$\Gamma(K^{*0} \rightarrow K^0 \gamma)$	124.5	116.6	124.5	116.6	117 ± 10
$\Gamma(K^{*+} \rightarrow K^+ \gamma)$	79.5	71.4	79.5	71.4	50 ± 5

TABLE V. Radiative decay widths $\Gamma(P \rightarrow \gamma \gamma)$ obtained by using the axial anomaly plus PCAC relations. $\theta_{SU(3)} = -19^\circ$ for $\eta - \eta'$ mixing is used for both potential cases. The experimental data are taken from Ref.[17].

Widths	H.O.	Linear	Experiment
$\Gamma(\pi \rightarrow \gamma \gamma)$	7.73	7.84	7.8 ± 0.5 [eV]
$\Gamma(\eta \rightarrow \gamma \gamma)$	0.42	0.42	0.47 ± 0.05 [keV]
$\Gamma(\eta' \rightarrow \gamma \gamma)$	4.1	3.9	4.3 ± 0.6 [keV]

REFERENCES

- [1] S. Godfrey and N. Isgur, Phys. Rev. D **32**, 189(1985).
- [2] M. V. Terent'ev, Yad. Fiz. **24**, 207(1976) [Sov.J. Nucl. Phys. **24**, 106(1976)]; V. B. Berestetsky and M. V. Terent'ev, *ibid.* **24**, 1044(1976) [**24**, 547(1976)]; **25**, 653(1977)[**25**, 347(1977)].
- [3] Z. Dziembowsky and L. Mankiewicz, Phys. Rev. Lett. **58**, 2175(1987); Z. Dziembowsky, Phys. Rev. D **37**, 778(1988).
- [4] C.-R. Ji and S.R. Cotanch, Phys. Rev. D **41**, 2319(1990); C.-R. Ji, P.L. Chung and S.R. Cotanch, Phys. Rev. D **45**, 4214(1992).
- [5] H.-M. Choi and C.-R.Ji, Nucl. Phys. A **618**, 291(1997).
- [6] W. Jaus, Phys. Rev. D **41**, 3394(1990).
- [7] W. Jaus, Phys. Rev. D **44**, 2851(1991).
- [8] P.L. Chung, F. Coester, and W.N. Polyzou, Phys. Lett. B **205**, 545(1988).
- [9] H.-M. Choi and C.-R.Ji, Phys. Rev. D **56**, 6010(1997).
- [10] T.Huang,B.-Q. Ma,and Q.-X.Shen, Phys.Rev.D **49**, 1490(1994).
- [11] F.Schlumpf, Phys.Rev.D.**50**, 6895(1994).
- [12] F. Cardarelli *et al.*, Phys. Lett. B **349**, 393(1995); **359**, 1(1995); **332**, 1(1994).
- [13] C.-R. Ji and S.J. Rey, Phys. Rev. D **53**, 5815(1996).
- [14] Y. Kuramashi *et al.*, Phys. Rev. Lett. **72**, 3448(1994).
- [15] C.-R.Ji and Y.Surya, Phys.Rev. D **46**, 3565(1992).
- [16] D.E.Soper, ph.D. Thesis, SLAC Report No. 137 (1971).
- [17] Particle Data Group, R. M. Barnett *et al.*, Phys. Rev. D **54**, 1(1996).
- [18] A. De Rújula, H. Georgi, and S. Glashow, Phys. Rev. D **12**, 147(1975).
- [19] N. Isgur, Phys. Rev. D **12**, 3770(1975); **13**, 122(1976).
- [20] M. D. Scadron, Phys. Rev. D **29**, 2076(1984).
- [21] W.Lucha, F.F.Schöberl, and D. Gromes, Phys. Rep. **200**, 127(1991).
- [22] N. Isgur and G. Karl, Phys. Lett. B **72**, 109(1977).
- [23] D. Gromes and I. O. Stamatescu, Nucl. Phys. B **112**, 213(1976).
- [24] N. Isgur, D. Scora, B. Grinstein, and M. B. Wise, Phys. Rev. D **39**, 799(1989).
- [25] D. Scora and N. Isgur, Phys. Rev. D **52**, 2783(1992).
- [26] S. Capstick and N. Isgur, Phys. Rev. D**34**, 2809(1986).
- [27] T. Das, V. S. Mathur, and S. Okubo, Phys. Rev. Lett. **19**, 470(1967); J. J. Sakurai, *ibid.* **19**, 803(1967).

- [28] R. J. Oakes and J. J. Sakurai, Phys. Rev. Lett. **19**, 1266(1967).
- [29] S. Coleman and H. J. Schnitzer, Phys. Rev. **134**, B863(1964); N. M. Kroll, T. D. Lee, and B. Zumino, *ibid.* **157**, 1376(1967).
- [30] C. J. Bebek *et al.*, Phys. Rev. D **17**, 1693(1978).
- [31] J. J. Sakurai, K. Schilcher and M. D. Tran, Phys. Lett. B **102**, 55(1981); J. S. Bell and J. Pasupathy, *ibid.* B **83**, 389(1970).
- [32] R. A. Amendolia *et al.*, Phys. Lett. B **178**, 435(1986).
- [33] J. F. Donoghue, B. R. Holstein, and Y. C. R. Lin, Phys. Rev. Lett. **55**, 2766(1985).
- [34] *The second DAΦNE physics handbook*, edited by L. Maiani, G. Pancheri, and N. Paver, published 1995 by INFN-LNF- Divisione Ricerca, ISBN 88-86409-02-8.
- [35] F. Anulli *et al.*, *Measurement of two photon interactions with the KLOE small angle tagging system*, p. 607 in Vol. II of Ref. [34].
- [36] CELLO Collaboration, H.-J.Behrend *et al.*, Z. Phys. C **49**, 401(1991).
- [37] CELLO Collaboration, V.Savinov *et al.*, Report No. hep-ex/9507005.
- [38] TPC/2 γ Collaboration, H.Aihara *et al.*, Phys. Rev. Lett. **64**, 172(1990).
- [39] private communication with Prof. Nathan Isgur.

FIGURES

Fig.1(a). The central potential $V_0(r)$ versus r . Our Coulomb plus harmonic oscillator(solid line) and linear(dotted) potentials are compared with the quasi-relativistic potential of ISGW2 [25] model with $\kappa = 0.3$ (long-dashed line) and $\kappa = 0.6$ (dot-dashed line) and the relativized potential of GI [1] model(short-dashed line).

Fig.1(b). The central force $f_0(r)$ versus r . Our force for the linear potential is the same as that of ISGW2 with $\kappa = 0.3$ (dotted lines). The forces of GI and ISGW2 with $\kappa = 0.6$ are the same with each other(dashed lines). Our force for the harmonic oscillator potential(solid line) are quite comparable with the other four forces up to the range of $r \lesssim 2$ fm.

Fig.2(a). The variational principle satisfying Eq.(A2). The solid, dotted, and dot-dashed lines are fixed by the sets of $(m_u, \beta_{u\bar{u}})$, $(m_s, \beta_{u\bar{s}})$, and $(m_s, \beta_{s\bar{s}})$, respectively.

Fig.2(b). The variational principle satisfying Eq.(A3). The same line codes are used as Fig.2(a).

Fig.3. The charge form factor for the pion compared with data taken from Ref. [30]. The solid and dotted lines correspond to the results of harmonic oscillator and linear potential cases, respectively.

Fig.4(a). Theoretical predictions of charged K^+ form factors using the parameters of both harmonic oscillator(solid) and linear(dotted) potentials compared with a simple two-pole VMD model [31](dot-dashed), $F_{K^+(K^0)}^{\text{VDM}} = e_{u(d)}m_\omega^2/(m_\omega^2 + Q^2) + e_{\bar{s}}m_\phi^2/(m_\phi^2 + Q^2)$.

Fig.4(b). Theoretical predictions of neutral K^0 form factors. The same line codes are used as Fig.4(a).

Fig.5. The decay rate for the $\pi \rightarrow \gamma^*\gamma$ transition obtained from the one-loop diagram. Data are taken from Refs. [36,37].

Fig.6. The decay rate for the $\eta \rightarrow \gamma^*\gamma$ transition obtained from the one-loop diagram. Data are taken from Refs. [36–38].

Fig.7. The decay rate for the $\eta' \rightarrow \gamma^* \gamma$ transition obtained from the one-loop diagram. Data are taken from Refs. [36–38].

Fig.1(a)

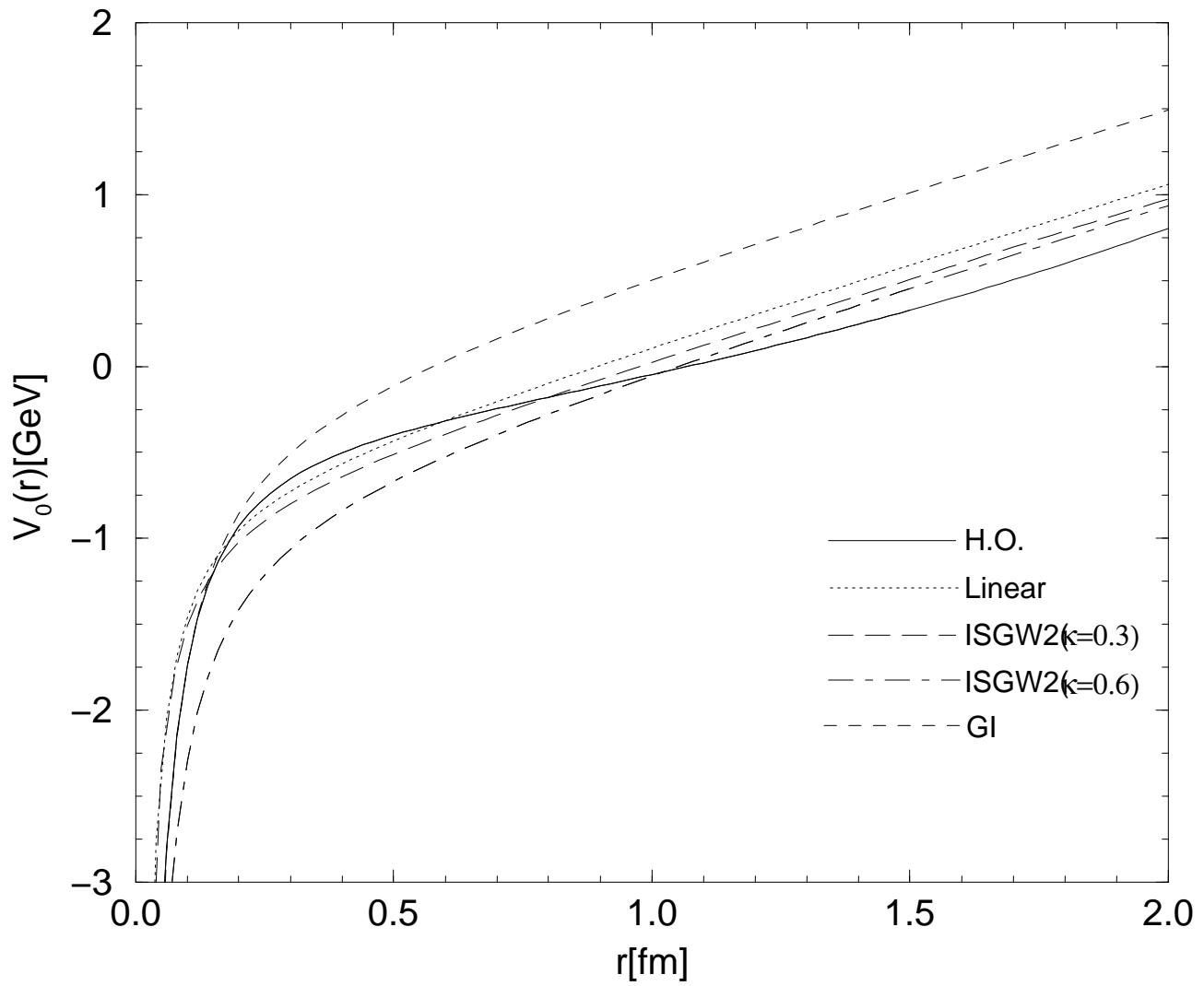


Fig.1(b)

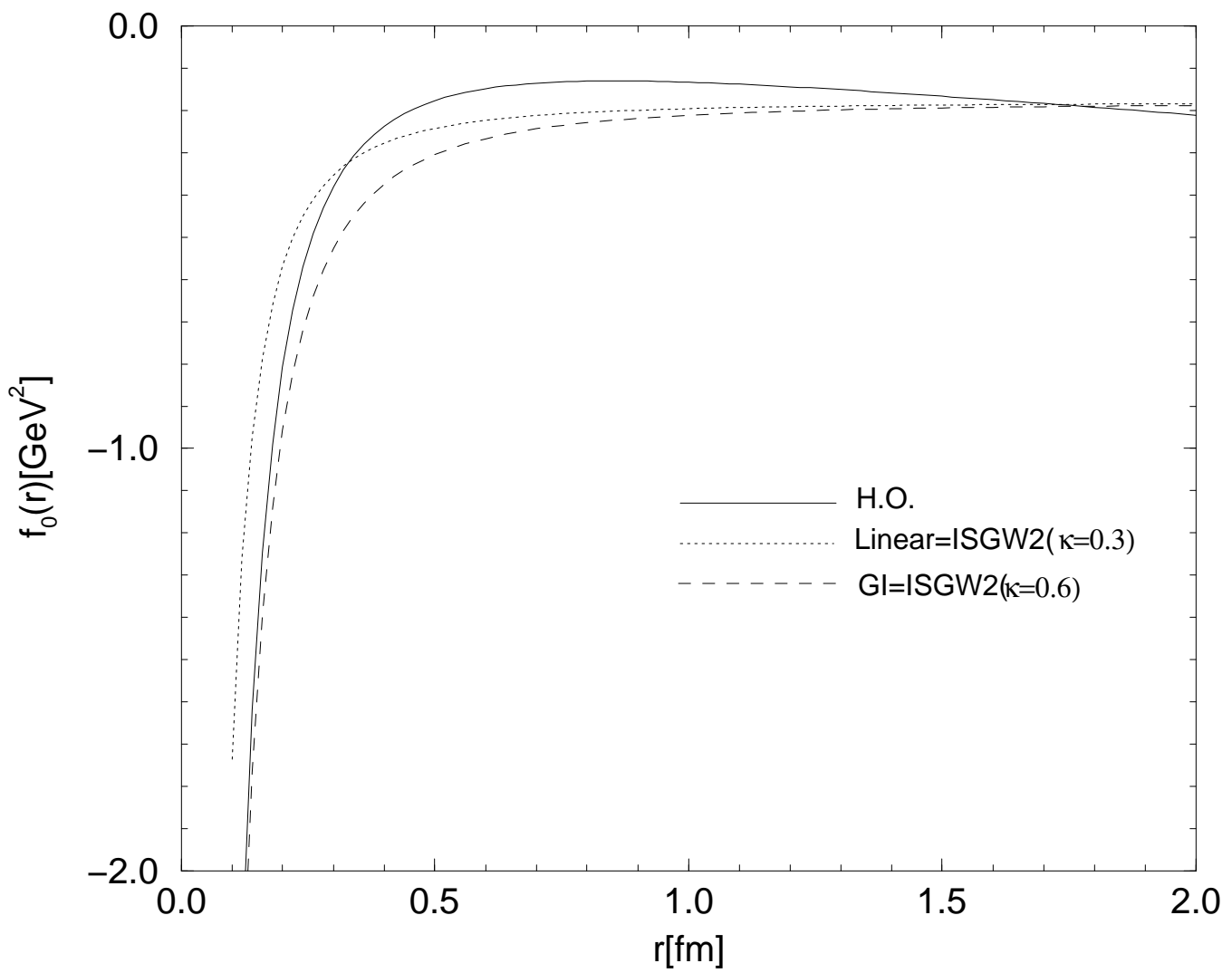


Fig.2(a)

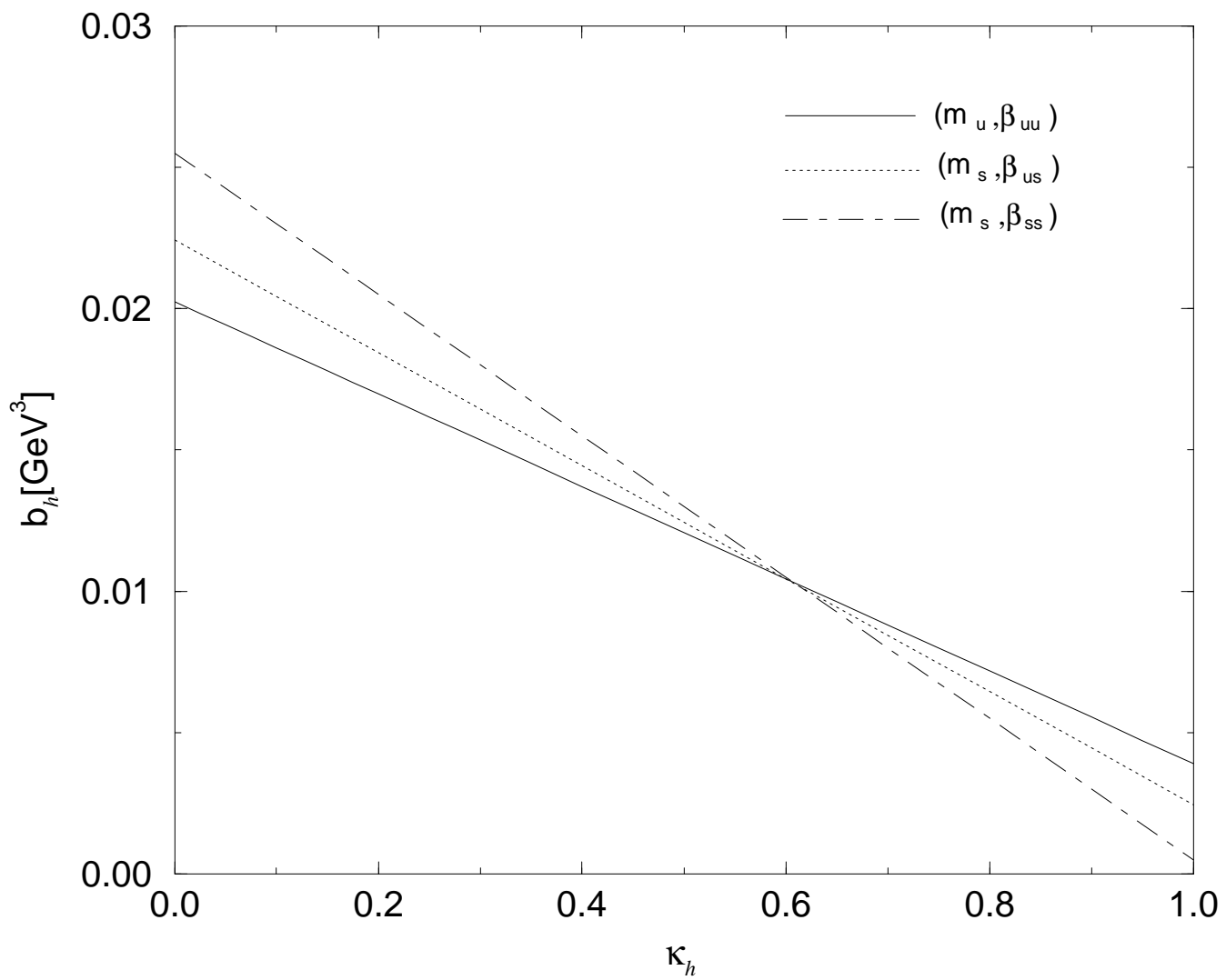


Fig.2(b)

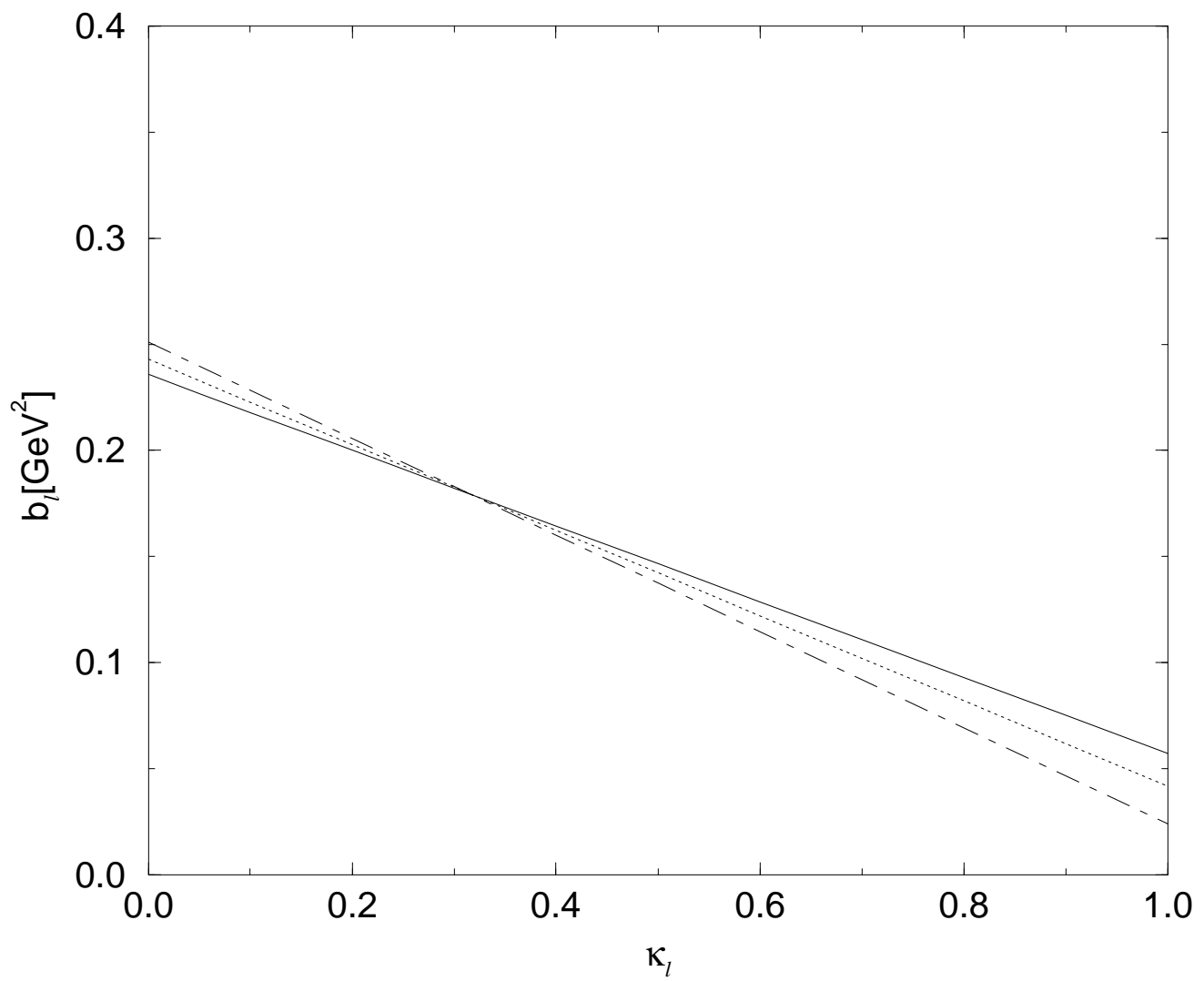


Fig.3

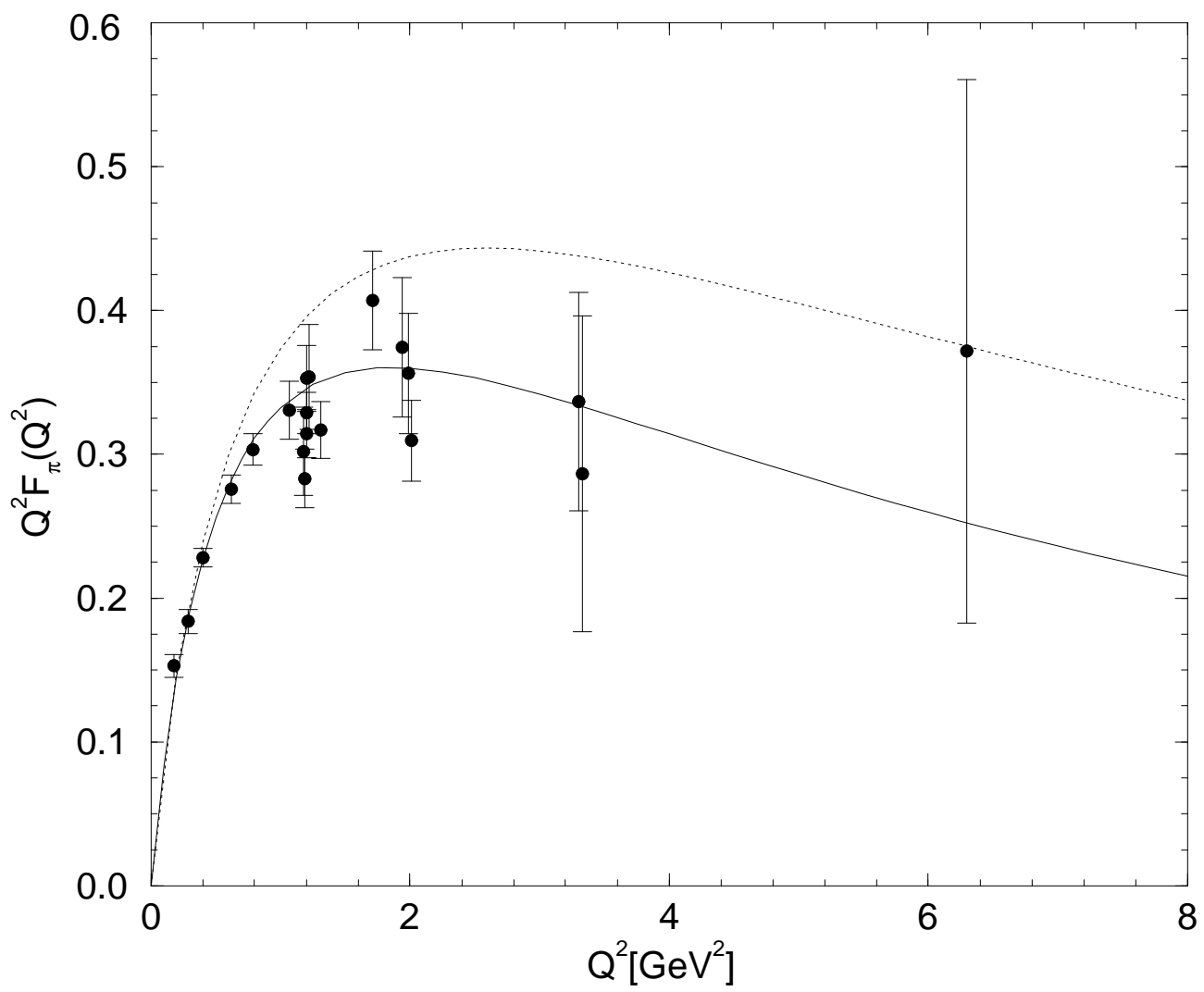


Fig.4(a)

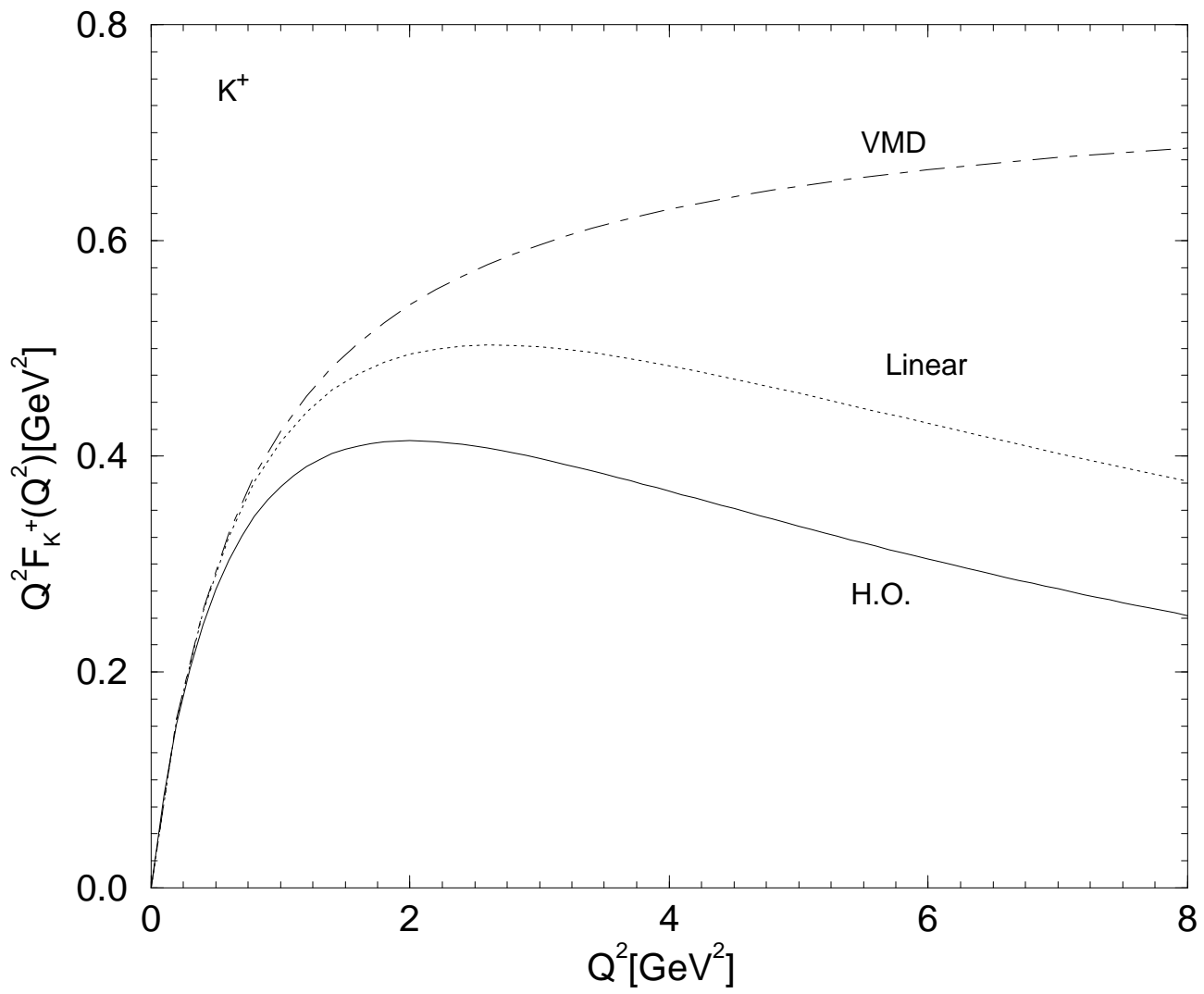


Fig.4(b)

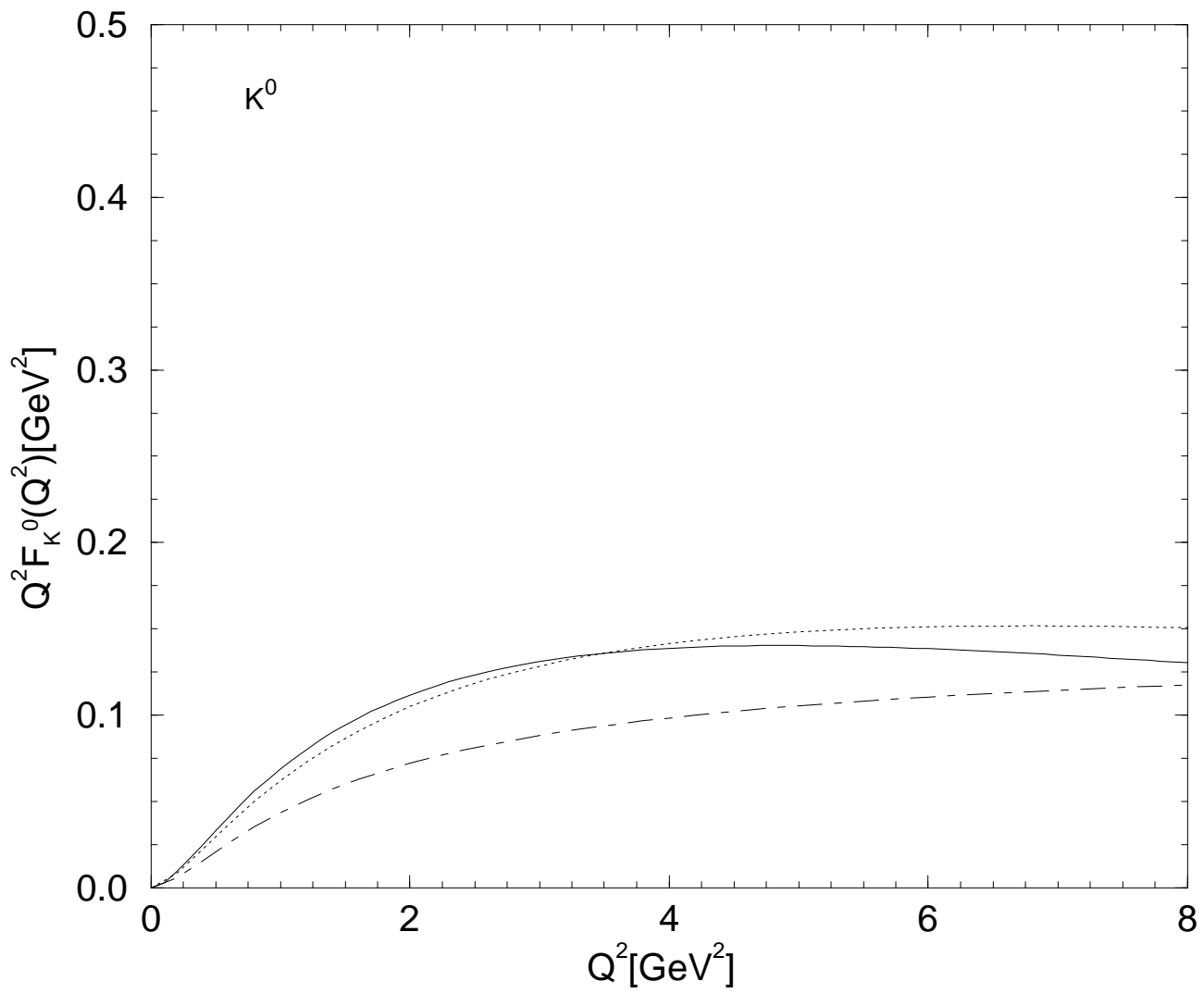


Fig.5

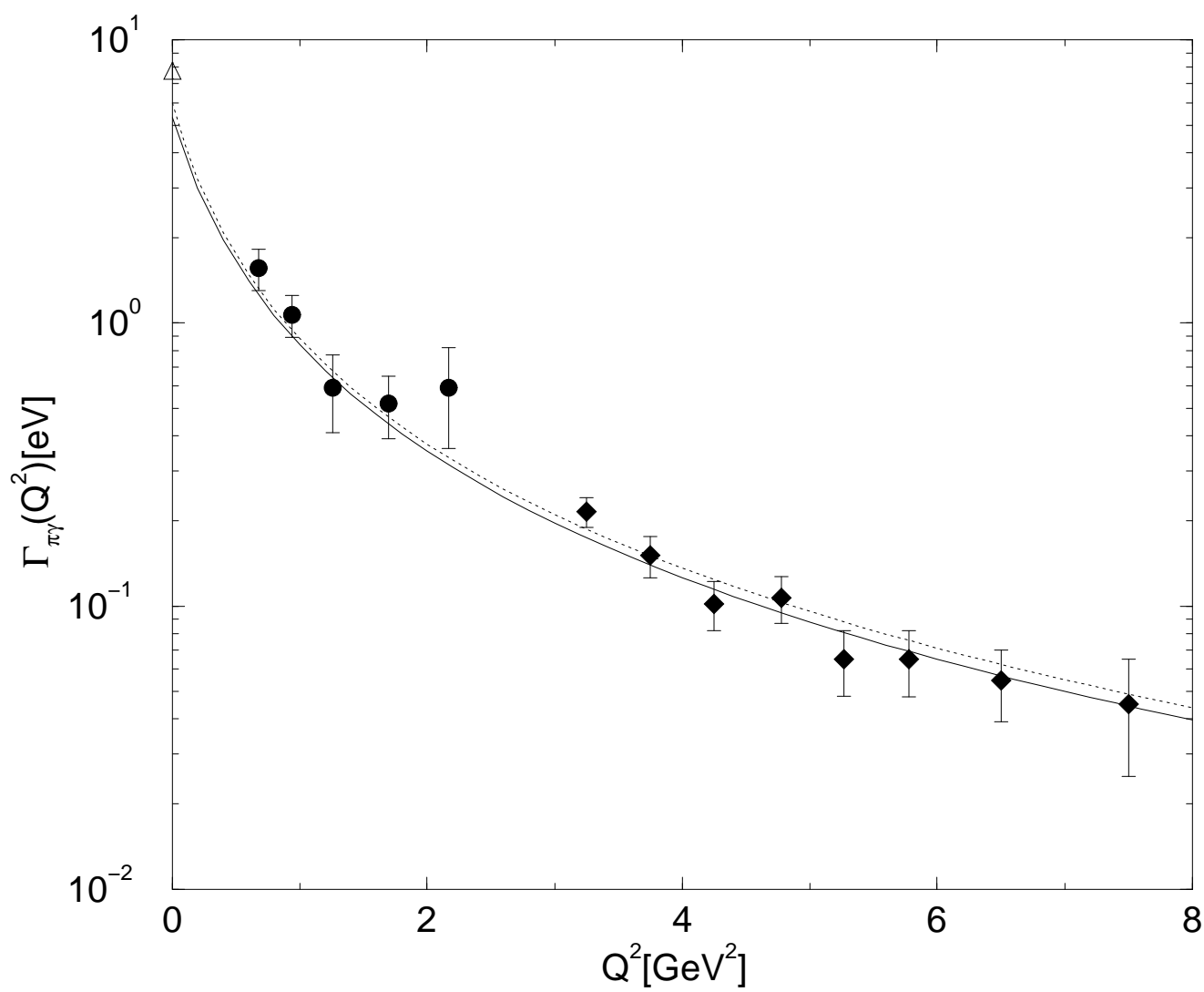


Fig.6

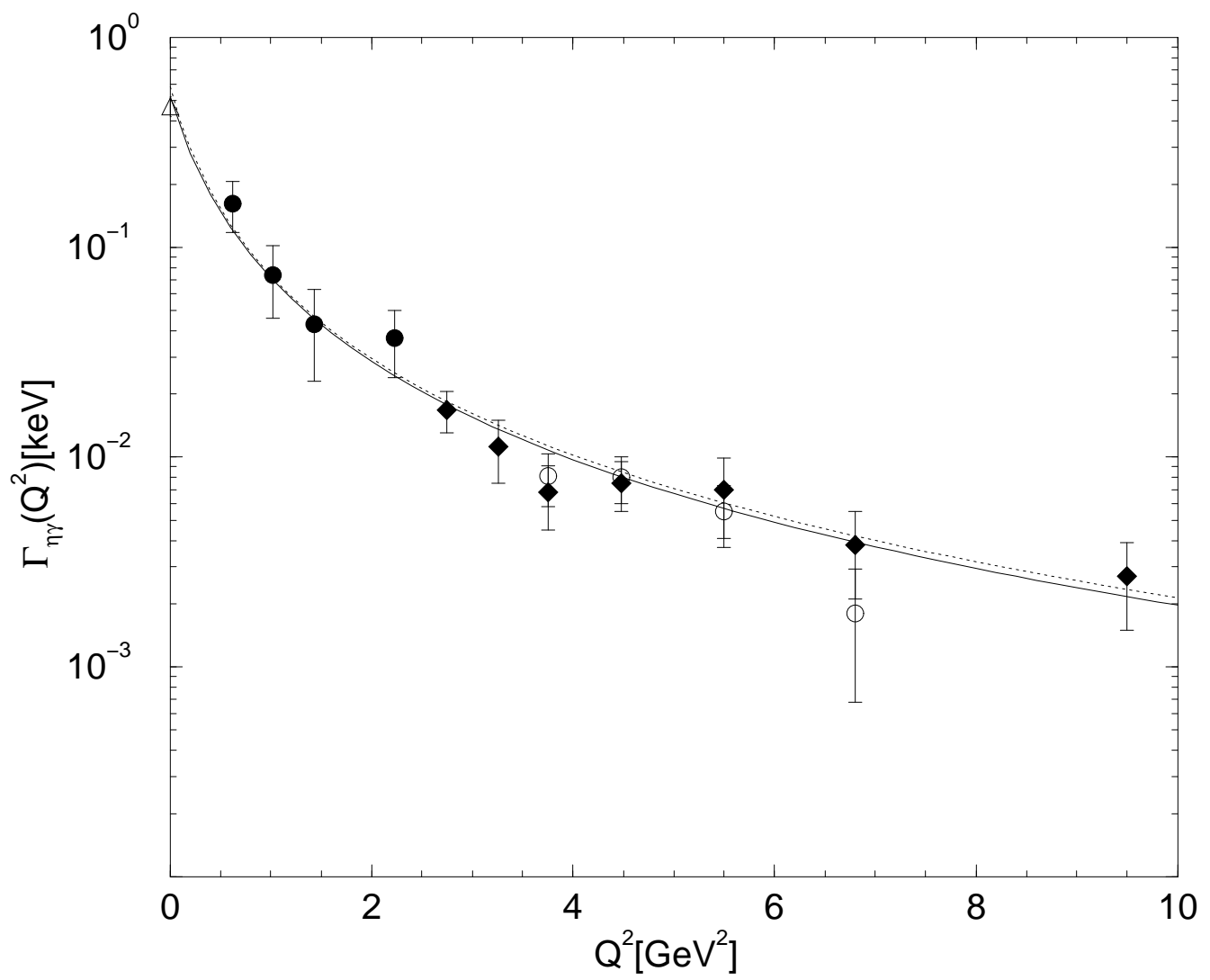


Fig.7

